RESEARCH ARTICLE

Reaction Engineering, Kinetics and Catalysis

Quantitative principle of shape-selective catalysis for a rational screening of zeolites for methanol-to-hydrocarbons

Mingbin Gao[1] ⓘ | Hua Li[1] ⓘ | Junyi Yu[1,2] | Mao Ye[1] ⓘ | Zhongmin Liu[1,2]

[1]National Engineering Research Center of Lower-Carbon Catalysis Technology, Dalian Institute of Chemical Physics, Chinese Academy of Sciences, Dalian, China

[2]University of Chinese Academy of Sciences, Beijing, China

Correspondence
Mao Ye and Zhongmin Liu, National Engineering Research Center of Lower-Carbon Catalysis Technology, Dalian Institute of Chemical Physics, Chinese Academy of Sciences, Dalian 116023, China.
Email: maoye@dicp.ac.cn and liuzm@dicp.ac.cn

Abstract

The production of hydrocarbons for the synthesis of readily available energy and multifunctional materials is of great importance in modern society. Zeolites have proven to be a boon for the targeted regulation of specific hydrocarbon as shape-selective catalyst in converting carbon resources. Yet our mechanistic understanding and quantitative description of shape-selectivity of zeolite catalysis remains rather limited, which restricts the upgrade of zeolite catalysts. Herein, we proposed quantitative principle of shape-selectivity for zeolite catalysis using methanol-to-hydrocarbons (MTH) as model. Combining with molecular simulations and infrared imaging, we unveil the competition of thermodynamic stability, preferential diffusion and favored secondary reactions between different hydrocarbons within zeolite framework are the essence of zeolite shape-selective catalysis. Notably, we provide methodology to *in silico* search for the optimal combination of framework topology and acidity properties of zeolites with operating conditions that potentially outperform commercial MTH catalysts to achieve high selectivity of desired hydrocarbon products.

KEYWORDS
diffusion, kinetics, methanol-to-hydrocarbons, shape-selective catalysis, zeolites

1 | INTRODUCTION

Zeolites with large topological diversity are versatile microporous mineral materials.[1,2] The typical applications of zeolite have proven to be a boon for, but not limited to, industrial catalysis,[3,4] chemical separation[2] and environments.[1] In modern society, the synthesis of two main necessities, readily available energy (e.g., liquid fuel) and diversiform multifunctional materials (e.g., plastics), predominantly relies on the hydrocarbon feedstocks.[5] As shown in Figure 1A, one of particularly important applications of zeolites being chemical catalysis to generate hydrocarbons with multiple carbon sources, such as fluid catalytic cracking (FCC) of crude oil,[3] hydrogenation of CO₂, methanol-to-hydrocarbons (MTH),[4,6,7] and syngas-to-olefins reactions[2] using coal or biomass as raw material. The success and enormous economic importance of zeolite as material catalyze is mainly attributed to its unique shape selectivity.[5,6,8–10]

The historical definition of shape selectivity is that the product distribution will deviate from the ideal thermodynamic distribution if the generated molecules is inhibited by the constraints on molecular size and shape imposed by the nanometer-sized space within materials.[5] Following this concept, implement of zeolite catalyst with appropriate framework or microenvironments (e.g., type and density of heteroatom embedded in framework) can achieve targeted regulation of specific hydrocarbon products.[11] The conversion of industrially relevant MTH reaction using zeolite is regarded as a prototypical shape-selective catalysis as shown in Figure 1B. Theoretically, the thermodynamic distribution of interconvertible olefin products in gas phase is inclined to propylene and butene.[12] Modulation of zeolite framework topology can give rise to the directed control of hydrocarbons distribution.[13–21] Empirically, in Figure 1B, products of MTH reactions may be gasoline mixture (MTG)/propylene (MTP) catalyzed by zeolites with medium-/large-pore or light olefins (MTO) catalyzed by zeolites with small-pore. Exploiting shape selectivity of zeolite catalyst has gained great success for almost 60 years and still expanding its applications,[2] yet
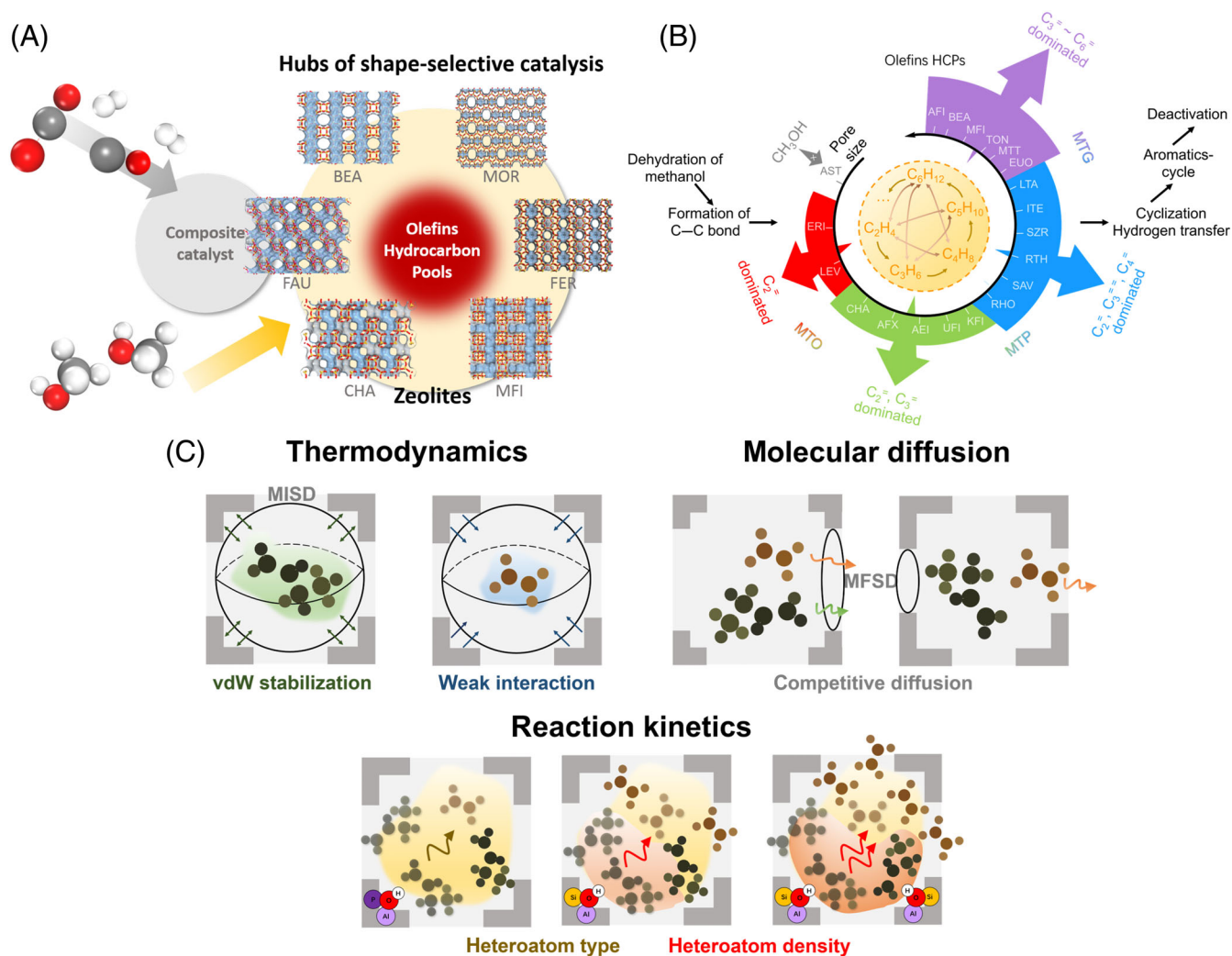
FIGURE 1 (A) Zeolite materials as industrial catalyst or composite catalyst to product specific distribution of hydrocarbons from multiple carbon sources. (B) Overview of the reaction mechanism of MTH and the implement of zeolite framework topology to regulate distribution of hydrocarbon products for MTH reactions. (C) Basic effects underlying shape selectivity, that is, competition of thermodynamics, molecular diffusion and reaction kinetics between different hydrocarbon species controlled by zeolite framework topology and heteroatom embedded in framework. MISD, the maximum included sphere diameter; MFSD, the maximum free sphere diameter

molecular mechanistic understanding remains rather limited especially at quantitative level.[5]

Consideration of three basic effects underlying shape selectivity,[5] such as space-constraint of reaction intermedia and diffusion-limitation of reactant or products, can give a good indication of which products are likely to form in qualitatively. Currently, enormous endeavors are undertaken to construct relation between free-energy landscape of reaction intermediates and zeolite topology from perspective of thermodynamics.[5,13,21] Taking the n-decane hydroconversion as an example, Smit et al.[5] obtained stable structure of isomer-decane intermedia within different zeolite frameworks by configurational-bias Monte Carlo simulations. Through pyrolysis mechanism combined with predominated isomer intermedia within specific zeolite framework, the preferential split products can be screened. For MTH reactions catalyzed by aromatics ensembled within zeolite, hepta-methylbenzenium cation (7MB+) is served as

intermediate to product propylene and butylene, while penta-methylbenzenium cation (5MB+) is served as intermediate to product ethylene and propylene. By use of density functional theory (DFT) calculations, Ferri et al.[14,15,22] defined the ratio $E_{int(7/5)}$ of interaction free energy between 7MB+ and 5MB+ to quantify relative stability between 7MB+ and 5MB+ within zeolite framework. Using the parameter $E_{int(7/5)}$ as key descriptor, they preliminarily found selectivity ratio of propylene to ethylene is proportion to value of $E_{int(7/5)}$. Parallelly, Kang et al.[13,20] defined cage-defining ring (CDR) to evaluate spaced size provided for the alkylation reaction of aromatics within zeolites. The formed alkyl-side chain of aromatics within framework with large CDR is usually longer than that within framework with small CDR. They found that as the dimension of CDR increases, the predominated products vary from ethylene, propylene to butylene. Such thermodynamic "free-energy landscape" approach can estimate highly-probable reaction intermedia formed within zeolite framework

and corresponding products with high possibility, which can partially elucidate shape selectivity imposed by zeolite framework without consideration of detailed chemical characteristics of framework[5] and molecular diffusion-limitation. The application of "free-energy landscape" approach is rather limited when reaction pathways are simple and the effect of kinetic factor (e.g., competition of reaction pathway and diffusion between species) can be ruled out. The impact of zeolite framework (e.g., void size and heteroatom of framework) on intrinsic reaction kinetics reflects on the stability of transition states imposed by the confined microenvironments. For the competitive reactions between isomerization and β-scission of alkanes, by use of DFT calculations, Noh et al.[23] found that void size of zeolite framework (Al-MCM-41, FAU, SFH, BEA, MFI) cannot significantly differentiate stability of transition states of isomer-heptane. They demonstrated that discrepant product selectivity within different zeolites arise from intracrystalline diffusivity of precursors for secondary β-scission reaction. Essentially, they stressed that the product selectivity is determined by the coupling between reactivity and molecular diffusive properties of zeolite catalysts. Deluca et al.[24] found that hydrogenation free-energy barriers are generally similar for two aluminosilicate frameworks (i.e., H-SSZ-13 and HZSM-5), while free-energy barriers for hydrogenation reactions in phosphoaluminosilicate framework (H-SAPO-34) are significantly higher than those in aluminosilicates. This implies that heteroatom type embedded in zeolite framework has prominent role in determining reaction kinetics. For zeolite framework decorated with various type of heteroatom, Studt et al.[25,26] summarized the linear scaling relations between the transition-state enthalpies of methylation reaction and adsorption enthalpy of ammonia, which illustrates that heteroatom type can regulate microenvironments within zeolite (e.g., acid site strength) and control the reaction kinetics. Through advanced microscopy imaging[27,28] and the-state-of-the-art simulation techniques,[29–35] tremendous efforts have been made to construct and understand the relation between molecular diffusivity and zeolite framework structure (e.g., the maximum included sphere diameter (MISD) and maximum free sphere diameter (MFSD)[36]) under non-reaction condition. Molecular diffusion-limitation imposed by zeolites plays a crucial role in determining characteristics of shape selectivity.[5,15,37,38] However, constructing straightforward relationship between products selectivity and molecular diffusion remains a big challenge, which is inhibited by the complicated reaction kinetics under reaction conditions. As discussion above, the essence of shape selectivity of zeolite catalysis can be ascribed to the competition of thermodynamics, reaction kinetics and molecular diffusion between species confined within framework. Advances in separated influence of zeolite framework on thermodynamics, reaction kinetics and molecular diffusion has achieved, however, comprehensive modeling or theory integrated above three factors is still lacking and remains elusive.[5,8,39] There are three major challenges to construct quantitative shape selectivity for zeolite catalysis. For the complexed reaction network, it is difficult to refine intrinsic kinetic constant of essential reaction step as descriptors to represent microenvironment of zeolite. Extracting intrinsic relation of thermodynamics/intracrystalline diffusivity between key molecules

and zeolite framework using concise descriptors. It is critical of assembly of descriptor involved thermodynamics, reaction kinetics and molecular diffusion within confined zeolite framework to the physicochemically-straightforward formula of product selectivity, which is beneficial to construct a reliable-ideally quantitative-principle for shape selectivity of zeolite catalysis.

Here we present a quantitative principle of shape selectivity for zeolite catalysis using MTH reactions as model reaction. Such modeling can serve as the rational design and *in silico* screen of zeolite catalysts that are particularly suitable for production of desired hydrocarbons. The quantitative principle of shape selectivity is validated by available experimental data of MTH reactions catalyzed by zeolites with diverse topologies, type and density of heteroatom embedded in frameworks under different temperature. Moreover, combining quantitative modeling of shape selectivity with advanced infrared microscope (IRM) and *ab initio* molecular dynamics (AIMD), the essential principle of zeolite shape selectivity is clearly elucidated at molecular-level. We believe that the proposed mechanism of shape selectivity and prediction of hydrocarbons selectivity on the basis of a quantitative principle of shape selectivity can be a widely applicable approach for zeolite catalyst and illuminate the way to zeolite shape-selective catalysis.

1.1 | Theoretical formalism of shape selectivity for MTH reactions catalyzed by zeolite

Theoretical formalisms of shape selectivity for zeolite catalysis are derived using MTH reactions as model. Typically, the reaction course of MTH reaction can be segmented into induction period (formation of hydrocarbon pool species, HCPs), high-efficiency sustainment (autocatalysis by HCPs), and decay (coke deactivation).[11] Taking the quasi-stable state of MTH reactions to construct theoretical formalisms, that is, autocatalysis stage, which can simplify the complication and dynamic evolutions of process. For the autocatalysis stage, the formation of hydrocarbons from methanol reacted with Brønsted acid sites (BAS) and HCPs can be simplistically represented as

$$\text{MeOH} + [\text{HCPs} - \text{BAS}] \xrightarrow{k_1} \frac{1}{y}\text{C}_y^= + \text{H}_2\text{O}, \tag{1}$$

$$\text{MeOH} + [\text{HCPs} - \text{BAS}] \xrightarrow{k_2} \frac{1}{2}\text{C}_2^= + \text{H}_2\text{O}, \tag{2}$$

$$\text{C}_y^= + [\text{BAS}] \xrightarrow{k_{\text{C}_y^=}} \frac{y}{2}\text{C}_2^=, \tag{3}$$

$$\text{C}_2^= + [\text{BAS}] \xrightarrow{k_{\text{C}_2^=}} \frac{2}{y}\text{C}_y^=, \tag{4}$$
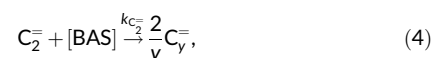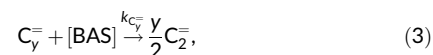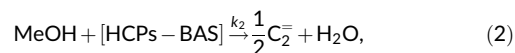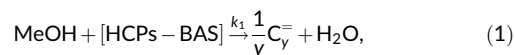
where k is the reaction kinetic constant, [HCPs-BAS] the HCPs (olefinic or aromatic species) combined with BAS within zeolite framework, $\text{C}_2^=$ the ethylene and $\text{C}_y^=$ ($y = 3, 4, 5, 6$ in this work) the propylene, butylene, pentene and hexene products, respectively. The theoretical formalisms of shape selectivity are developed based on

binary components to represent the competitive relationship between $C_\gamma^=$ and $C_2^=$ within zeolite framework. Based on the reaction step shown in Equations (1)–(4), corresponding partial differential equations of reaction–diffusion modeling are shown in Equations (S1)–(S3), second type boundary conditions of zeolite crystal shown in Equations (S4)–(S6) and reactor model shown in Equations (S7)–(S9). Based on both the experimental[27,40] and simulations[41] evidences, it has been indeed recognized that the intracrystalline diffusion and surface barriers are two dominant mechanisms controlling pore entrance resistance in zeolites. Intracrystalline diffusion is mainly controlled by the topology of zeolite framework, type of guest molecules, temperature and loading of molecules. In an early effort, we developed a correlation between the intracrystalline diffusivity of guest molecules and geometry of zeolite framework[33] (Equations S42–S46). However, surface barriers, which can be dominated by various factors, would be affected not only by the zeolite framework topology[41] and type of guests,[40] but also the external surface properties and environment of exposure.[42] In the current work, as the preliminary step toward the reaction–diffusion model accounting for the mass transfer mechanism, we focused on the intracrystalline diffusion and treated it as the dominant mechanism of mass transfer in order to simplify the reaction–diffusion model. For the multicomponent adsorption on the zeolite surface, ideal adsorbed solution theory (IAST)[43] is employed. The derived analytical solutions of intracrystalline concentration C of $C_\gamma^=$ and $C_2^=$ products within zeolite catalyst are given in Equations (S10)–(S11) (detailed derivations can refer to Supplementary Note 1). The ratio of selectivity between $C_\gamma^=$ and $C_2^=$ in gas phase is defined as

$$\frac{Sel_{C_\gamma^=}}{Sel_{C_2^=}} = \frac{C_{C_\gamma^=}^{gas}}{C_{C_2^=}^{gas}} = \frac{D_{C_\gamma^=} C_{C_\gamma^=}|_{x=l}}{D_{C_2^=} C_{C_2^=}|_{x=l}}, \quad (5)$$

where Sel is the selectivity of hydrocarbon products, C^{gas} the concentration of hydrocarbons in gas phase, D the intracrystalline diffusivity and l the half length of the zeolite crystal. The concise and physically-significant form of Equation (5) can be rewritten to Equation (6) (see the detailed derivations in Supplementary Note 1)

$$\frac{Sel_{C_\gamma^=}}{Sel_{C_2^=}} = \frac{D_{C_\gamma^=}}{D_{C_2^=}} \left(\frac{2}{\gamma} \frac{D_{C_2^=} k_1}{D_{C_\gamma^=} k_2} \right) \frac{\left(\frac{C_{C_\gamma^=}|_{x=l}}{C_{C_2^=}|_{x=l}} \right)}{\left(\frac{2}{\gamma} \frac{D_{C_2^=} k_1}{D_{C_\gamma^=} k_2} \right)} = \frac{2}{\gamma} \frac{k_1}{k_2} f(D,k)$$

$$= K\left(C_2^= \leftrightarrow C_\gamma^=\right) \left(\frac{D_{C_\gamma^=}}{D_{C_2^=}} \right)^{\eta_y}. \quad (6)$$

The term of $\frac{2}{\gamma} \frac{k_1}{k_2}$ can be approximated to the chemical equilibrium constant $K\left(C_2^= \leftrightarrow C_\gamma^=\right)$ when olefin species as dominated HCPs. While aromatic species are served as dominated HCPs, aromatic species can be used as addition catalytic cycle for methanol to product olefins, the deviation in chemical equilibrium between olefin species will occur. Therefore, the applicability of Equation (6) is mainly suitable for olefin species as dominated HCPs. Chemical equilibrium constant can be calculated by $K\left(C_2^= \leftrightarrow C_\gamma^=\right) = \exp\left(\Delta S\left(C_2^= \leftrightarrow C_\gamma^=\right)/R \right) \exp\left(\Delta H\left(C_2^= \leftrightarrow C_\gamma^=\right)/RT \right)$,

where ΔH $(C_2^= \leftrightarrow C_\gamma^=)$ is the enthalpy change and ΔS $(C_2^= \leftrightarrow C_\gamma^=)$ the entropy change between $C_\gamma^=$ and $C_2^=$ within zeolite framework. The calculation method and the value summary of ΔH $(C_2^= \leftrightarrow C_\gamma^=)$ and ΔS $(C_2^= \leftrightarrow C_\gamma^=)$ in various zeolite framework are introduced in Supplementary Note 9 and Table S17, respectively. In Figure S24, under ideal chemical equilibrium between olefin species, the predominate olefin products formed in zeolite catalyst are propylene and butene. In additional, owning to the van der Waals stabilization of olefin species with long chain $C_\gamma^=$ imposed by zeolite framework, it can be noticed that the selectivity of $C_\gamma^=$ formed in zeolite catalyst is higher than that formed in gas phase. This reflects the significant role of adsorption thermodynamics controlled by framework topology, which is mainly depended on the characteristic dimension of MISD.[13,21] In this work, the MISD of involved zeolite is large than 0.60 nm, which can ensure the interactions between specific olefin and different frameworks are similar (Tables S15 and S16).

In the Equation (6), the term of $\frac{2}{\gamma} \frac{D_{C_2^=} k_1}{D_{C_\gamma^=} k_2}$ represents the ratio of intracrystalline concentration between $C_\gamma^=$ and $C_2^=$ when the formation of olefin products is through the parallel reactions by methanol reacted with [HCPs-BAS], that is, Equations (1) and (2). The term of $\frac{C_{C_\gamma^=}|_{x=l}}{C_{C_2^=}|_{x=l}}$ represents the ratio of intracrystalline concentration between $C_\gamma^=$ and $C_2^=$ when the interconversion between $C_\gamma^=$ and $C_2^=$, that is, Equations (3) and (4), are taken into consideration. Thus, the ratio of $\left(\frac{C_{C_\gamma^=}|_{x=l}}{C_{C_2^=}|_{x=l}} \right) / \left(\frac{2}{\gamma} \frac{D_{C_2^=} k_1}{D_{C_\gamma^=} k_2} \right)$, which is defined as function $f(D,k)$, reflects the effect of competitive diffusion and β-scission reaction between $C_\gamma^=$ and $C_2^=$ on the ratio of intracrystalline concentration $\frac{C_{C_\gamma^=}|_{x=l}}{C_{C_2^=}|_{x=l}}$. As shown in Figure S2, as the discrepancy of intracrystalline diffusivity between $C_\gamma^=$ and $C_2^=$ enlarges (i.e., the ratio of $D_{C_\gamma^=}/D_{C_2^=}$ decreases), the value of $f(D,k)$ significantly decreases, which implies that molecular sieving effect imposed by MFSD of zeolite framework impedes the diffusion of large olefins $C_\gamma^=$ and enhances the β-scission reaction of $C_\gamma^=$ into small molecule $C_2^=$. In addition, the correlation between $f(D,k)$ and $D_{C_\gamma^=}/D_{C_2^=}$ shows power function relation, that is, mathematical formalism of $f(D,k) = \left(D_{C_\gamma^=}/D_{C_2^=} \right)^\eta$. On the other hand, increasing kinetic constant $k_{C_\gamma^=}$ also results in the decrease in $f(D,k)$, which implies that improving β-scission reaction kinetics of $C_\gamma^=$ can effectively promote cracking of $C_\gamma^=$ into small molecule $C_2^=$. In particular, the parameter η shows strong relation with kinetic constant $k_{C_\gamma^=}$. Here, we define parameter η_y as the ratio of effectiveness factor of β-scission reaction between $C_\gamma^=$ ($y = 3, 4, 5, 6$) and $C_3^=$ (selecting effectiveness factor of propylene as benchmark),[44,45]

$$\eta_y = \frac{\eta_{C_\gamma^=}}{\eta_{C_3^=}} = \sqrt{\left(\frac{k_{C_3^=}}{k_{C_\gamma^=}} \frac{D_{C_\gamma^=}^{SS}}{D_{C_3^=}^{SS}} \right)_0} = \sqrt{\left(\frac{k_{C_3^=}}{k_{C_\gamma^=}} \frac{D_{C_\gamma^=}^{gas} K_{C_\gamma^=}^{chem}}{D_{C_3^=}^{gas} K_{C_3^=}^{chem}} \right)_0 \frac{C_{H^+}}{C_{H^+}^0}}, \quad (7)$$

where D^{SS} is the effective steady-state diffusivity,[46] D^{gas} the diffusivity in gas phase, $K_{C_\gamma^=}^{chem}$ the equilibrium constant of chemisorption at BAS, $C_{H^+}^0$ the referenced density of BAS ($C_{H^+}^0 = 1 \, mmol \, g_{cat.}^{-1}$), C_{H^+} the density of BAS (which reflects the density of heteroatom embedded

in zeolite framework) and subscript "0" represents the open space without confinement. Taking aluminum-substituted silica (Al-zeo.) and silica-substituted aluminophosphate (SAPO) 10T model (shown in Figure S3) to simulate intrinsic kinetics and chemisorption at BAS with different acid strength in open space. As summarization in Tables S2 and S4, the Equation (7) can be simplified to the form

$$\eta_y = \xi_{H^+}(\delta_y)_{Al-zeo.}\left(\frac{C_{H^+}}{C_{H^+}^0}\right)^{0.5}, \tag{8}$$

where ξ_{H^+} is the relative acid strength using aluminum-substituted silica as criterion, which is defined as $\xi_{H^+} = \Delta H_{ads}(NH_3@X)/\Delta H_{ads}(NH_3@Al-zeo.)$, where X is the zeolite framework decorated with different heteroatom (see Tables S5–S8) and the values of $(\delta_y)_{Al-zeo.}$ are 1.00, 0.70, 0.33, and 0.23 for $y = 3, 4, 5,$ and 6, respectively.

Besides interconversion between $C_y^=$ and $C_2^=$ as dominated secondary reactions, hydrogen transfer reaction of olefins to alkane needs to be taken into consideration. The simplified reaction of hydrogen transfer can be written into two steps[47]:

$$C_y^= + [BAS] \xrightarrow{k_{C_y^=}^{HS}} C_y^+, \tag{9}$$

$$C_y^= + C_y^+ \xrightarrow{k_{C_y^=}^{HT}} C_y^+ + C_y^0, \tag{10}$$
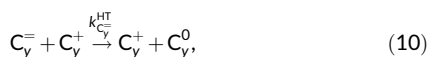
where C_y^+ is the carbocation of $C_y^=$, $k_{C_y^=}^{HT}$ the kinetic constant of hydrogen transfer of $C_y^=$ and $k_{C_y^=}^{HS}$ the kinetic constant of hydrogen shift of $C_y^=$. The ratio of selectivity between C_y^0 and $C_y^=$ ($y = 2, 3, 4, 5, 6$) can be calculated by (derivations are shown in Supplementary Note 1)

$$\frac{Sel_{C_y^0}}{Sel_{C_y^=}} = \frac{D_{C_y^0}C_{C_y^0}|_{C_{H^+}}}{D_{C_y^=}C_{C_y^=}|_{C_{H^+}^0}} = \frac{k_{C_y^=}^{HT}}{k_{C_y^=}^{HS}}\frac{C_{H^+}}{C_{H^+}^0} = \xi^2\left(\frac{k_{C^=}^{HT}}{k_{C^=}^{HS}}\right)_{Al-zeo.}\frac{C_{H^+}}{C_{H^+}^0}, \tag{11}$$

where $\left(k_{C^=}^{HT}/k_{C^=}^{HS}\right)_{Al-zeo.} = \exp\left(\Delta G_{Al-zeo.}^{HS} - \Delta G_{Al-zeo.}^{HT}/RT\right)$, $\Delta G_{Al-zeo.}^{HS} - \Delta G_{Al-zeo.}^{HT}$ can be approximated to 52.4 kJ mol^{-1} (Table S3). In Equation (11), for the olefins and alkanes with the same carbon number, the intracrystalline diffusivity $D_{C_y^0}$ and $D_{C_y^=}$ is assumed to be similar.

The quantitative formalism Equation (6) of shape selectivity for MTH reactions catalyzed by zeolite can be intuitively interpreted that products distribution of hydrocarbons deviates from the thermodynamic equilibrium, which is resulted from the competition of molecular diffusion and secondary reactions between hydrocarbon species. Combining Equation (6) with Equation (8) can determine the ratio of selectivity between $C_y^=$ and $C_2^=$, and using Equation (11) can determine the ratio of selectivity between alkane and alkene. As shown in Figure 2, experimental data of MTH reactions catalyzed by zeolites with different framework topology, for example, AFI,[48] TON,[16] MTT,[16] LTA,[13,19] RHO,[13] ITE,[13,14] SZR,[16] RTH,[13,14] SAV,[13,19] KFI,[13] UFI,[13] AEI,[13,14] AFX,[19] CHA,[13,14] LEV,[13] and ERI,[13,50] and heteroatom

embedded in framework (Al-zeo. and SAPO) at reaction temperature range of 623–773 K (Figures S17–S19) were used to validate the developed model. The normalized root-mean-square errors between predicted and experimental results of $Sel_{C_3^=}/Sel_{C_2^=}$, $Sel_{C_4^=}/Sel_{C_2^=}$, $Sel_{C_5^=}/Sel_{C_2^=}$, $Sel_{C_6^=}/Sel_{C_2^=}$, and $Sel_{C_y^0}/Sel_{C_y^=}$ are 0.27, 0.39, 0.99, 0.54, and 0.35, which demonstrates the good precision of predictions by Equations (6) and (11). In the following, the molecular mechanisms of shape selectivity of zeolite catalysis for MTH reactions are further revealed based on the developed modeling combined with molecular dynamic simulations and advanced spectroscopy.

2 | EXPERIMENTAL AND SIMULATIONS

2.1 | DFT calculations

The intrinsic reaction kinetics of β-scission, hydrogen transfer and chemical sorption in open space at zeolite type and AlPO$_4$-based molecular sieves were obtained by 10T cluster model. The free energy barriers for each elementary reaction at 673 K were obtained from the ωB97XD/6-31G (d, p) total electronic energies and the thermal correction from the ωB97XD/6-31G (d, p): AM1 frequency calculations. Thermodynamic properties have been calculated in the framework of harmonic oscillator rigid rotator approximation.[51] In the search of transition state structure, QST3 method was used. DFT were performed using the Gaussian 09 package. Periodic DFT calculations were performed using the Perdew–Burke–Ernzerhof (PBE) exchange-correlation functional within the generalized gradient approach (GGA), as implemented in the CASTEP module implemented in Material Studio package (Accelrys Software).[18,25,51] The simulation details are introduced in Supplementary Note 2.

2.2 | Molecular dynamics simulations

The intracrystalline diffusivities of binary mixtures of C$_2$H$_4$/n-C$_4$H$_8$ or C$_2$H$_4$/n-C$_6$H$_{12}$ in zeolite frameworks were obtained from force field molecular dynamics (FFMD) simulations, which were not considered the effect of BAS interaction.[52] FFMD simulations were carried out using the Forcite in Materials Studio package[53] (see Supplementary Note 3). *Ab initio* MD (AIMD) simulations yield an improved description of olefin species-BAS interactions, although at higher computational cost.[32] The regular AIMD simulations were carried out with the CP2K simulation package (version 7.1)[54] (see Supplementary Note 4, the situation of BAS distribution within framework is also introduced).

2.3 | *In situ* infrared microimaging

The experiments were performed by use of a Fourier transform IR microscope (Bruker Hyperion 3000) composed of a spectrometer (Bruker vertex 70v) and a 15× optical microscope.[27] The *in situ* optical
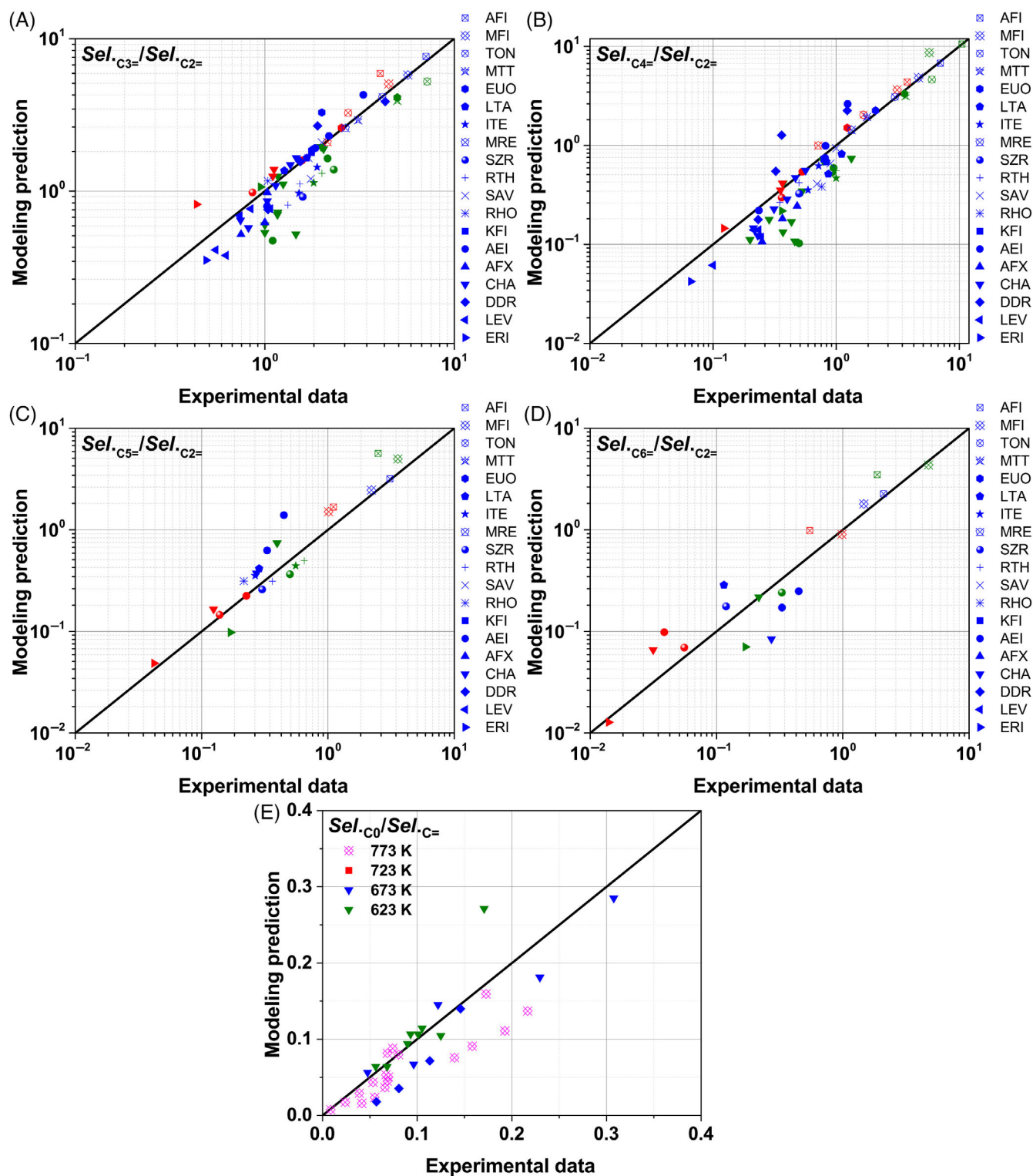
FIGURE 2 The selectivity ratio of (A) propylene to ethylene, (B) butylene to ethylene, (C) pentene to ethylene, (D) hexene to ethylene, and (E) alkane to alkene for MTH reactions catalyzed by zeolite catalyst with frameworks of AFI,[48] MFI, TON,[16] MTT,[16] EUO,[16] LTA,[13,19] ITE,[13,14] MRE,[16] SZR,[16] RTH,[13,14] SAV,[13,19] RHO,[13] KFI,[13] AEI,[13,14] AFX,[19] CHA,[13,14] DDR,[49] LEV,[13] and ERI[13,50] and different heteroatom embedded in framework at 623, 673, 723, and 773 K

reaction cell with BaF_2 window in this device is connected to a reactant system and mounted on a movable platform under the microscope (see Supplementary Note 7). The main functions of IR microscopy are detection of IR spectrum of bulk materials and/or spatial-resolved IR spectrum of local region of materials. In this work, we detected the IR spectrum of bulk materials by IR microscopy.
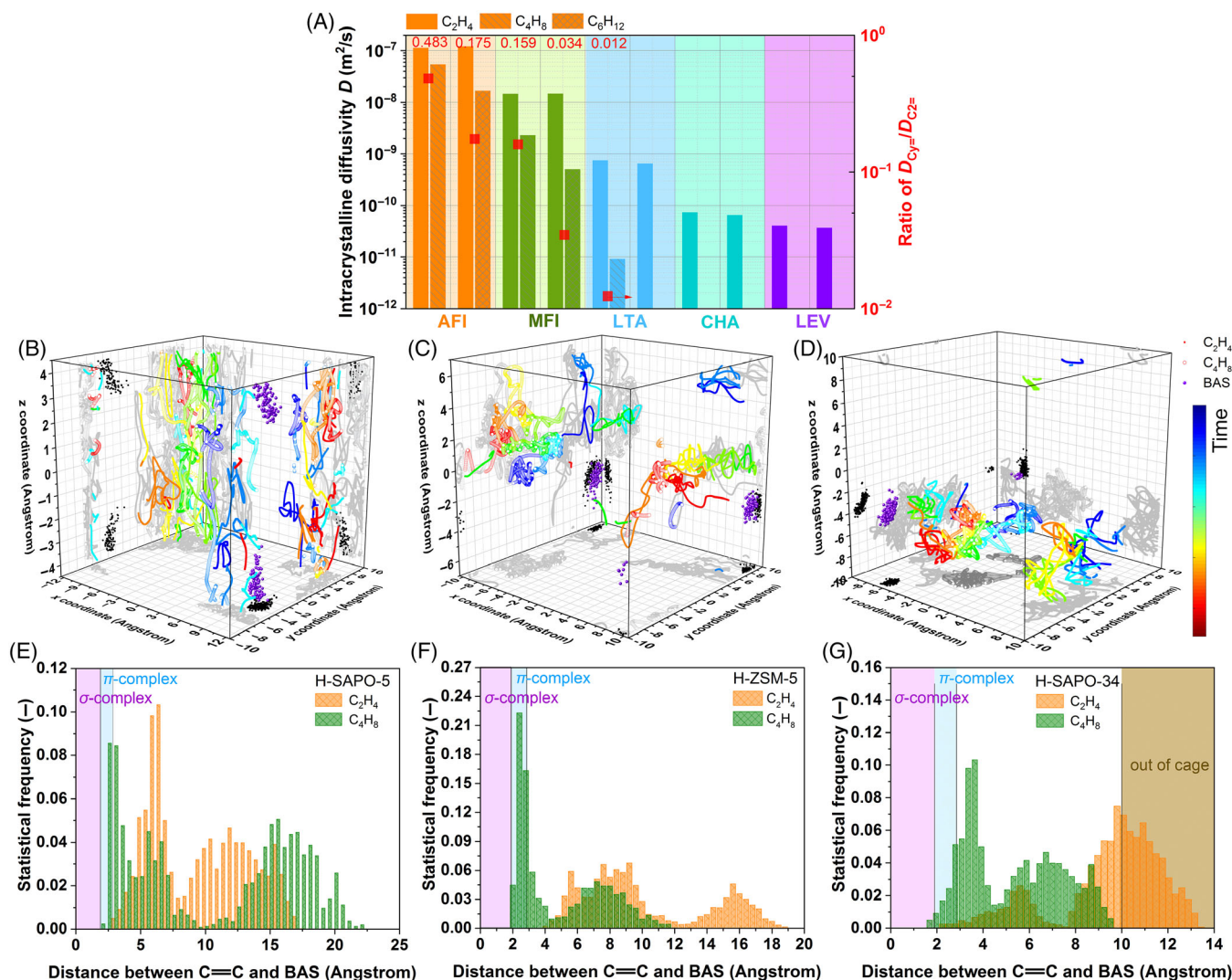
FIGURE 3 (A) Intracrystalline diffusivities of binary olefins of C_2H_4/C_4H_8 and C_2H_4/C_6H_{12} within AFI, MFI, LTA, CHA, and LEV frameworks at 673 K by FFMD simulations. Typical motion trajectories of C_2H_4 and C_4H_8 within (B) H-SAPO-5, (C) H-ZSM-5, and (D) H-SAPO-34 molecular sieves by AIMD. Corresponding statistical results of physisorbed and chemisorbed interaction between olefins and BAS in (E), H-SAPO-5, (F), H-ZSM-5, and (G) H-SAPO-34 molecular sieves

3 | RESULTS AND DISCUSSION

3.1 | Competitive diffusion between binary hydrocarbons within zeolite frameworks

As above discussion, the dimension of MISD of zeolite framework can significantly affect the van der Waals stabilization of guest molecules and thus control hydrocarbon products from perspective of thermodynamics. Hydrocarbons formed within zeolite framework subsequently need to diffuse through the nanosized window in succession into gas phase. In this section, the crucial role of featured window size, MFSD, in sieving hydrocarbons by controlling competitive diffusion between binary hydrocarbons is elaborated. In Equation (6), we defined the ratio $D_{C_y^=}/D_{C_2^=}$ to quantify competitive diffusion between binary olefins within zeolite framework. As shown in Figure S22, using Equations (S42)–(S46)[33] to predict the ratio $D_{C_y^=}/D_{C_2^=}$ in different

zeolite framework, as MFSD decreases or carbon chain of olefins increase, the ratio $D_{C_y^=}/D_{C_2^=}$ shows significantly decrease. In addition, for the zeolite with small pore (e.g., MFSD <0.45 nm), as the chain of olefins increases, the value of $D_{C_y^=}/D_{C_2^=}$ sharply declines even subtle narrowing in MFSD. It is a non-trivial task to measure diffusivity of olefin species in zeolite at reaction temperature, which is resulted from the inevitable reactions between olefin species and BAS. In Table S14, the intracrystalline diffusivities of propane and n-butane under high temperature as possible (up to 473 K) were measured, and the predictions by Equations (S41)–(S45) are well consistent with experimental results. In Figure 3A, the intracrystalline diffusivities of ethylene, n-butene and n-hexene in binary components of C_2H_4/C_4H_8 and C_2H_4/C_6H_{12} loaded within AFI, MFI, LTA, CHA and LEV framework at 673 K were simulated by FFMD. As member of ring pores (MR) reduces, for example, AFI (12MR), MFI (10MR) and LTA (8MR), the ratio of $D_{C_4^=}/D_{C_2^=}$ and $D_{C_6^=}/D_{C_2^=}$ observably decreases, respectively.

In addition, the value of $D_{C_\gamma^=}/D_{C_2^=}$ simulated by FFMD is approximated to the predicted results as shown in Table S1, which validates the predicted accuracy of Equation (S42). For LTA framework, during simulation time (~5 ns), C_6H_{12} molecule hops form original cage to adjacent cage cannot be observed. Moreover, for zeolite framework with the same 8MR but slight distinction in MFSD, for example, LTA (~0.415 nm), CHA (~0.366 nm), and LEV (~0.347 nm), the diffusion behavior of olefins varies significantly. The intracrystalline diffusivity of C_2H_4 markedly declines as the MFSD decreases slightly. During simulation time (~5 ns), the diffusion of C_4H_8 and C_6H_{12} in CHA and LEV frameworks cannot be observed. Based on the results of FFMD and Figure S22, it can be concluded that MFSD of zeolite framework plays a decisive role in the distinction of molecular diffusion between different olefins. Crucially, decreasing MFSD can enhance competitive diffusion between olefin species and selectively extend residence time of hydrocarbons with long chain within zeolite framework. Herein, FFMD combined with predicted modeling, that is, Equation (S42), provide clear information about the effect of MFSD on molecular diffusion. However, for the real catalytic environment, the interaction between olefin species and BAS of framework needs to be further unveiled.

The regular AIMD yield an improved description of interaction between BAS and olefins.[32] The competitive diffusion behavior between binary components of C_2H_4/C_3H_6, C_2H_4/C_4H_8, C_2H_4/C_5H_{10}, and C_2H_4/C_6H_{12} loaded within zeolite framework of H-SAPO-5 (AFI), H-SSZ-24 (AFI), H-ZSM-5 (MFI), H-SAPO-34 (CHA), and H-SSZ-13 (CHA) and olefin-BAS interaction were simulated. For instance, for binary components of C_2H_4/C_4H_8 within AFI, MFI and CHA frameworks, the typical motion trajectories of olefins are shown in Figures 3B–D and S13a,c, corresponding statistical results of interaction between olefins and BAS are shown in Figures 3E–G and S13b, d. In Figure 3E–G, defining statistical frequency of distance between olefins and BAS to evaluate the molecular diffusion limitation imposed by framework decorated with BAS. Within limited simulation time (~50 ps), the frequency distributions in maximum distance between C_2H_4/C_4H_8 and BAS are similar in H-SAPO-5, as MR narrows, the frequency distribution in maximum distance between C_2H_4 and BAS is notably higher than that between C_4H_8 and BAS in H-ZSM-5. For the competitive diffusion between C_2H_4 and C_4H_8 within CHA framework, hopping event of C_4H_8 between adjacent cages of CHA framework cannot be captured during limited simulation time (~50 ps), which is similar with observation by FFMD. AIMD clearly reveals that framework confinement can regulate interaction between olefins and BAS. Compared with weak physisorbed state of olefins within H-SSZ-24 and H-SAPO-5 (12MR), 10MR of H-ZSM-5 enhances the probability of emergence of physisorbed π-complex of olefins $C_\gamma^=$ with long carbon chain, and H-SSZ-13 and H-SAPO-34 with 8MR even facilitate the emergence of chemisorbed alkoxide of $C_\gamma^=$. This implies that in zeolite framework with narrow pore window, diffusion limitation controlled by MFSD and acid site strength regulated by heteroatom type may favor the stabilization interaction between olefins with long chain and BAS. The MISD of CHA framework (H-SSZ-13) is similar to that of AFI framework (H-SSZ-24), but the MFSD of H-SSZ-13 (~0.366 nm) is significantly smaller than that of H-SSZ-24

(~0.736 nm), small MFSD of H-SSZ-13 notably increases the contact time between $C_\gamma^=$ and BAS owing to the strong diffusion limitation by the small MFSD. For the competitive diffusion between olefin species within H-SSZ-24/H-SAPO-5 and H-SSZ-13/H-SAPO-34, it can be found that increasing BAS strength can directly lead to enhanced probability of emergence of physisorbed π-complex and chemisorbed alkoxide of $C_\gamma^=$ within framework. Physisorbed π-complex and chemisorbed alkoxide species are considered to be precursors of β-scission and hydrogen transfer reactions of $C_\gamma^=$. AIMD simulations indicate that reducing MFSD not only facilitate competitive diffusion between olefin species but also selectively retard olefins with long chain within framework to interact with BAS and further secondary reactions. Combining MD simulations with predicted modeling, the competitive diffusion between olefin species involved in Equation (6) within zeolite frameworks decorated with different heteroatom is discussed in details.

3.2 | Secondary reactions of olefins controlled by zeolite framework

For the zeolite framework decorated with BAS, the MFSD not only controls the competitive diffusion between olefin species but also determines the degree of secondary reactions, for example, β-scission. Assuming chemical equilibrium between $C_\gamma^=$ and $C_2^=$ and ruling out the secondary reactions of olefin species, the ratio of intracrystalline concentration between $C_\gamma^=$ and $C_2^=$ can be represented as $K\left(C_2^= \leftrightarrow C_\gamma^=\right)\frac{D_{C_2^=}}{D_{C_\gamma^=}}$ in Equation (6). Under such assumption, the term $K\left(C_2^= \leftrightarrow C_\gamma^=\right)\frac{D_{C_2^=}}{D_{C_\gamma^=}}$ indicates that narrowing MFSD, that is, parameter $D_{C_2^=}/D_{C_\gamma^=}$ increases (see Figure S22), the ratio of intracrystalline concentration between $C_\gamma^=$ and $C_2^=$ increases. This can be interpreted that in zeolite framework with narrow pore window, olefins with long chain $C_\gamma^=$ are inclined to be trapped inside the framework. For the real catalytic conditions, the secondary reactions of olefin species cannot be ruled out. As shown in Figure 4A, as MFSD decreases, on the contrary, the ratio of intracrystalline concentration between $C_\gamma^=$ and $C_2^=$ decreases, which illustrates the occurance of intensive cracking reaction from $C_\gamma^=$ into $C_2^=$ within framework with small MFSD. Taking zeolite framework as a nano-reactor, at the initial moment, the chemical equilibrium between $C_\gamma^=$ and $C_2^=$ is approximated, nanosized-window can not only differentiate the diffusivity between olefin species but also make the ratio of intracrystalline concentration between $C_\gamma^=$ into $C_2^=$ deviate from chemical equilibrium. When the effect of MFSD on competitive diffusion between $C_\gamma^=$ and $C_2^=$ is indistinctive, the ratio of intracrystalline concentration between $C_\gamma^=$ and $C_2^=$ approaches to the $K\left(C_2^= \leftrightarrow C_\gamma^=\right)\frac{D_{C_2^=}}{D_{C_\gamma^=}}$, that is, the intracrystalline-dominated species is $C_\gamma^=$ according to the Figure S24. When MFSD of framework imposes significant diffusion competition between olefins, as well illustrated by FFMD and AIMD, the probability of formation of physisorbed π-complex and chemisorbed alkoxide of $C_\gamma^=$ enhances, which means that is the enhancement of cracking reaction from $C_\gamma^=$ into $C_2^=$. In this sense, preferential diffusion of small olefins $C_2^=$ through narrowed MFSD disturbs the chemical equilibrium between $C_\gamma^=$ and $C_2^=$ and promotes the
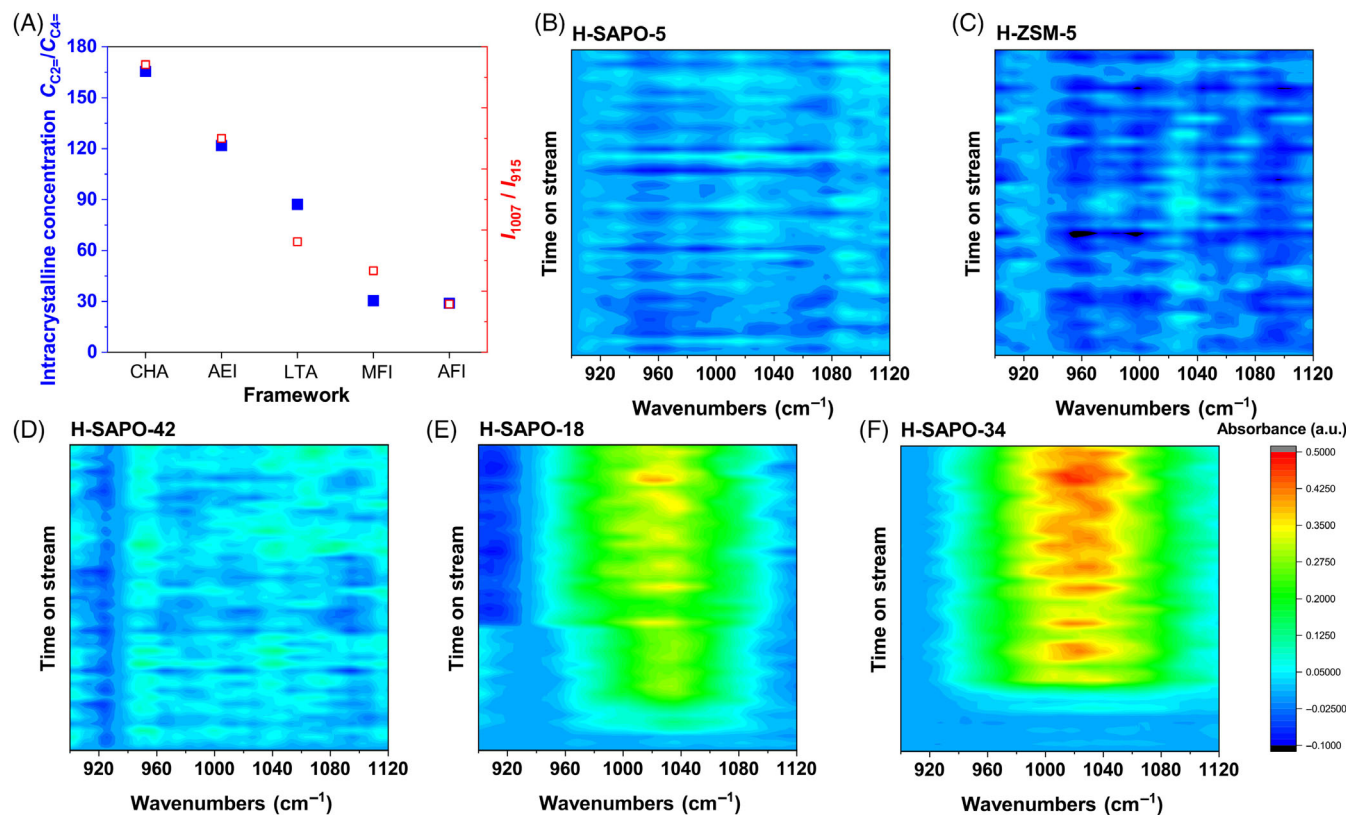
FIGURE 4 (A) The relative proportion between ethylene and olefins with long carbon chain within AFI, MFI, LTA, AEI, and CHA zeolite frameworks. *In situ* observations of subtractive IR signal of confined olefin species within (B) H-SAPO-5, (C) H-ZSM-5, (D) H-SAPO-42, (E) H-SAPO-18 and (F), H-SAPO-34 zeolites during MTH reactions by IRM at 673 K

cracking of $C_y^=$ to $C_2^=$. As shown in Figure 4A, based on the theoretical analysis by Equation (6) combined with AIMD, we can conclude that MFSD not only determines the preferential diffusion of olefins but also controls the degree of secondary reactions of olefins.

Figure 4A shows that decreasing the MFSD results in the decreased ratio of intracrystalline concentration between $C_y^=$ and $C_2^=$. Advanced IRM combined with diffuse reflectance infrared Fourier transform spectroscopy (DRIFTS) were implemented to validate the dominated intracrystalline olefins within bulk zeolites during initial-efficient stage of MTH reactions. AIMD simulations were first used to obtain characteristic IR fingerprint peak of olefin species confined within zeolite framework. In Figure S14, the wagging vibration of ethylene at ~1000 cm^{-1} presents intense and unique IR signal compared with other olefins, while the IR fingerprint peak of olefin species with long carbon chain shows wide distribution of IR signal at the range of 900–1100 cm^{-1}. Thus, using the wavenumbers around 900–1100 cm^{-1} as characteristic signal to identify the confined olefin species. However, the IR spectral at this region overlaps the intense modes from the zeolite framework. Before the inlet of methanol, no obvious changes in IR spectrum of framework were observed. Figure 4 presents the subtractive IR spectrum between formed olefins with zeolites and zeolite framework, which was assigned as the IR signal of olefin species formed within zeolite. As shown in Figure 4B–E, the MFSD follows the order: H-SAPO-5 (AFI, 0.736 nm) > H-ZSM-5

(MFI, 0.560 nm) > H-SAPO-42 (LTA, 0.415 nm) > H-SAPO-18 (AEI, 0.378 nm) > H-SAPO-34 (CHA, 0.366 nm). In Figure S21, after purging of catalyst surface by nitrogen, it can be noticed that the emerged characteristic IR signal at 900–1100 cm^{-1} during MTH reactions disappeared. Considering the slow mobility of aromatics within zeolite framework,[32] which are difficult to be removed from zeolite framework by nitrogen, it can assign characteristic IR signal at 900–1100 cm^{-1} to the olefin species. In Figure 4B–F, as MFSD decreases, it can be observed that the distinct increase in concentration of confined olefin species within framework. In Figure S21a–e of *in situ* DRIFT experiments, taking peak at ~1007 and ~913 cm^{-1} as IR fingerprint of ethylene and olefins with long chain, respectively. Defining ratio I_{1007}/I_{913} of relative signal strength at ~1007 and ~913 cm^{-1} to identify the relative proportion between ethylene and olefins with long chain. In Figure 4A, combing the calculated results by Equation (6) with *in situ* IR experiments, the enhancement of relative proportion of ethylene to olefins with long chain within framework as MFSD decreasing can be observed. These conclusions can be partly validated by UV-Raman spectroscopy.[55,56] Implementation of UV-Raman spectroscopy to MTH reactions shows that the ethylene is formed as a cracking product rather than the primary product.[55] In addition, decreasing the density of BAS of H-ZSM-5 would lead to the declination of ethylene.[55] Signorile et al.[56] found that zeolite with large MFSD enhances the diffusion of large olefins and
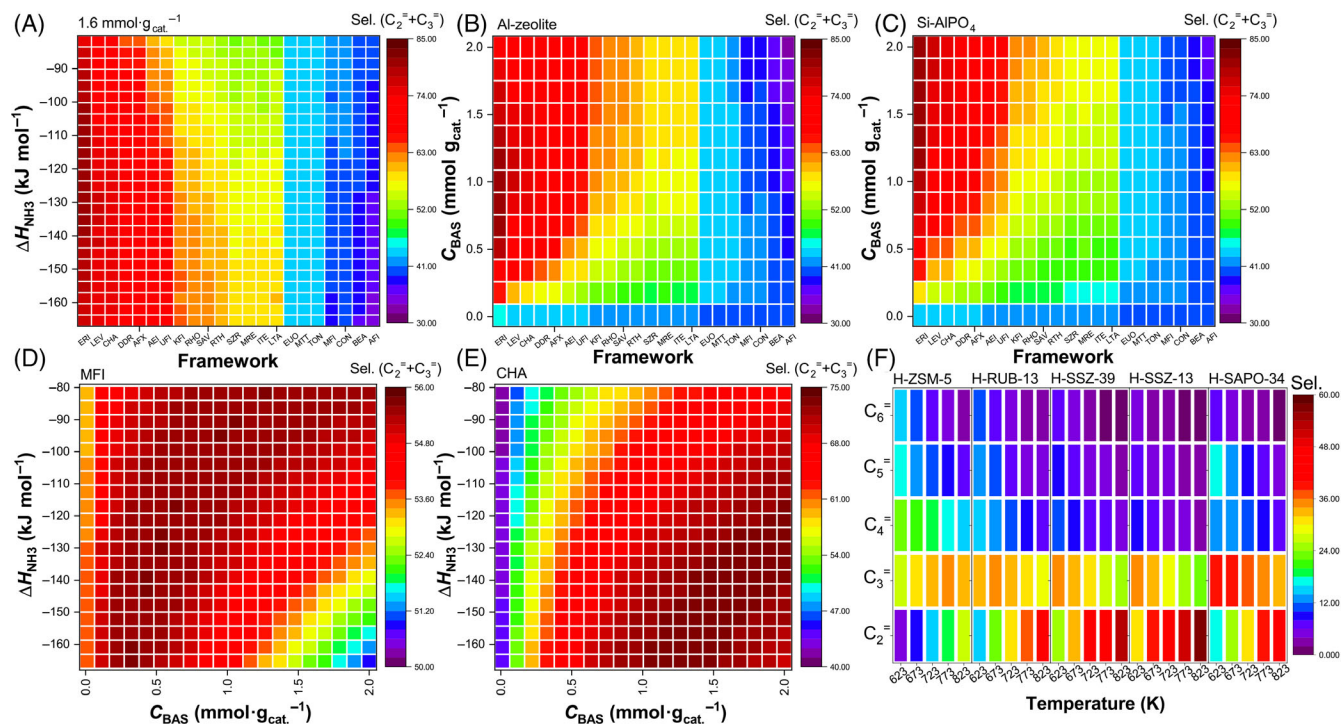
FIGURE 5 (A) The effect of BAS strength of zeolites with BAS density (1.6 mmol $g_{cat.}^{-1}$) and diverse framework on summing selectivity of ethylene and propylene (*Sel.* E + P) at 673 K. The effect of BAS density of (B) aluminosilicates and (C) silicoaluminophosphates with diverse framework on *Sel.* E + P at 673 K. The optimal range of BAS property of (D) MFI and (E) CHA zeolite frameworks for the optimized *Sel.* E + P at 673 K. (F) The effect of operating temperature of MTH reactions catalyzed by H-ZSM-5, H-RUB-13, H-SSZ-39, H-SSZ-13, and H-SAPO-34 zeolites on *Sel.* E + P

decreases the side reaction of large olefins by *operando* UV-Raman. Hereto, through Equation (6), MD simulations and *in situ* IRM experiments, the effect of shape selectivity on the competition of thermodynamics, secondary reactions, and diffusion between olefin species within framework are comprehensively illustrated.

3.3 | *In silico* screening and optimizations of zeolite catalysts for MTH reactions

Equation (6) integrates multidimensional structure descriptors of zeolite catalyst, for example, BAS strength ξ_{H^+}, BAS density C_{BAS}, and framework characteristic dimension of MISD and MFSD, competitive diffusion between olefins $D_{C_\gamma^=}/D_{C_2^=}$ and operating reaction temperature. In theory, *a priori*-predicted model Equation (6) can *in silico* reflect the effect of type and density of heteroatomic embedded in framework, framework topology and reaction conditions on hydrocarbons selectivity for MTH reactions, respectively. Figure 5A shows the impact of type of heteroatom embedded within diverse frameworks on summing selectivity of ethylene and propylene (*Sel.* E + P). For zeolite catalyst with small 8MR pores, for instance, zeolites with CHA or ERI framework, strong BAS property (e.g., H-SSZ-13,[14,15] MgAPO-34,[13] and H-SSZ-98[57]) is beneficial to the improvement of *Sel.* E + P, especially the promotion of ethylene formation (Figure S26). Inversely, for zeolites with 10 MR or 12 MR pores, for instance, zeolite with

MFI topology, weak BAS property (e.g., TaAlS-1,[58] [Al, B]-CON[59]) can enhance the production of ethylene and propylene, especially the formation of propylene (Figure S26). Al-zeo. and SAPO types are two most widely used zeolite catalysts,[15,21] the systematic investigations on the selectivity of hydrocarbons affected by BAS density of Al-zeo. and SAPO catalyst are shown in Figure 5B,C, respectively. For Al-zeo. with 8 MR pores, the suitable range of BAS density for optimization of *Sel.* E + P can be visualized in Figure 5B, which is evidenced by MTH reactions catalyzed by H-SSZ-98,[57] DDR zeolite,[49] and H-SSZ-13[60] with different BAS density. According to predicted results by Equation (6) shown in Figure 5B, excessively reducing BAS density of Al-zeo. catalyst with small pores will boost the formation of C_{4+} hydrocarbons, which is resulted from the impairment of the β-scission of C_{4+} species within framework. At the same framework, excessively increasing BAS density facilitates the events of hydrogen transfer reactions between olefins and BAS, which promotes the alkanes selectivity. For SAPO catalyst, inherent weak BAS property acts to the disadvantage of β-scission and hydrogen transfer reactions,[24] compared to the hydrocarbons selectivity from Al-zeo. catalyst with same framework and BAS density, the *Sel.* E + P of SAPO is usually lower than that of Al-zeo. as shown in Figure 5C. As indicated by Equation (6), to improve the *Sel.* E + P of SAPO catalyst, increasing BAS density and decreasing MFSD of framework can preferentially promote the cracking of olefins with long chain into low carbon olefins as evidenced by AIMD (Figure 4). For instance, synthesis of

H-SAPO-34[61] and H-SAPO-18[15] with suitable high BAS density can effectively improve the *Sel*. E + P while the selectivity of alkane is not significantly increases, which is also validated in Figure 5C. According to the Table S24, the formation of propylene and olefins with long chain from zeolite catalysts are favored in thermodynamics. Based on the Equation (6), as for Al-zeo. or SAPO catalysts with large pores, reducing the BAS density can suppress the cracking of olefins with high carbon number to ethylene and predominately promote the selectivity of propylene and olefins with long chain. On the contrary, appropriately increasing the BAS density combined with framework with narrowed MFSD can substantially raise selectivity of ethylene but accompanied with increased selectivity of alkanes.

MFI and CHA topologies are two widely used zeolite framework in industrial catalysis, despite enormous endeavors,[15,39] the construction of structure-performance descriptors as general optimization for zeolite catalysts is far from being achieved. In Figure 5D,E, non-linear relationship between *Sel*. E + P and BAS strength/density of MFI and CHA frameworks is clearly presented, respectively. For the optimization of *Sel*. E + P for H-SZM-5, the suitable BAS density is located at the range of 0.1–0.3 mmol $g_{cat.}^{-1}$, which implies that synthesis of H-ZSM-5 with low BAS density, that is, high Si/Al ratio, is potential to achieve this goal. Reducing BAS strength of MFI zeolite is also feasible route to attain optimal value of *Sel*. E + P. However, as indicated by Equation (6) and Figure 5D, properly increasing BAS density is necessary while reducing BAS strength. For example, incorporating tantalum into H-ZSM-5[58] to reduce BAS strength and properly increasing BAS density can effectively promote the selectivity of propylene, which is well predicted in Figures 5D and S29b. Similarly, such design role can be applied to zeolite catalyst with CHA framework, while high *Sel*. E + P is more facile to achieved due to the preferential diffusion of ethylene and propylene through small pores compared to the diffusion of olefins with long chain.

Reaction temperature is crucial factor in affecting hydrocarbons selectivity of MTH reactions. In Figure 5F, the hydrocarbons selectivity of typical zeolite catalysts at temperature range of 623–823 K are shown. Overall, increasing reaction temperature can facilitate the formation of ethylene and reduce selectivity of C_{4+} species due to thermodynamic advantage of cracking reactions (endothermic reaction) under elevated temperature. However, the dependence of temperature on propylene selectivity varies with the type of zeolite framework. Under high temperature, the thermodynamic stability of ethylene and propylene within zeolites is ascendant as indicated by Figure S24. For zeolite catalysts with large or medium pore, the effect of diffusion-limitation imposed by window of framework is not predominantly. Therefore, the relation between hydrocarbons selectivity and reaction temperature, to a great extent, depends on the thermodynamics, that is, *Sel*. E + P increases as reaction temperature increases. For small pores zeolite catalysts, due to the favor of β-scission under high temperature and diffusion limitation of olefins with long chain imposed by small pore, including propylene, which forces the olefins with long chain to be entrapped within framework and cracked into ethylene. In Figure 5F, the MFSD follows the order: H-RUB-13 (RTH, 0.408 nm) > H-SSZ-39 (AEI, 0.378 nm) > H-SSZ-13

(CHA, 0.366 nm), it can be observed that raising reaction temperature can significantly improve the ethylene selectivity of zeolite with decreasing 8MR pores. However, it needs to be noticed that increasing reaction temperature meanwhile promotes the hydrogen transfer reactions and enhances the alkane selectivity as indicated by Equation (11). As shown in Figure 5F, the optimal reaction temperature to achieve high selectivity of hydrocarbon products depends on the framework type and composition of zeolite catalysts. For the achievement of high *Sel*. E + P, the optimal temperature for zeolite with large or medium pores is suggested above 773 K, while the optimal temperature range for zeolite with small pores is 673–773 K. It is interesting to compare the optimal temperature for high *Sel*. E + P of H-SSZ-13 (673–773 K) and H-SAPO-34 (723–823 K) with the same framework but different framework composition. Due to the adverse nature of weak BAS property of H-SAPO-34 on hydrogen transfer reaction even at high temperature, the range of optimal temperature of zeolite catalyst with weak BAS property is wider than that of zeolite with strong BAS property.

In pursuit of a structure-performance relationship of zeolite catalysis for MTH reactions, a great number of experimental or theorical work toward the investigation of the effect of specific property of zeolites (e.g., BAS density of H-ZSM-5,[39,62] H-SAPO-18,[15] H-SSZ-13[21,60] and DDR[49] zeolite, BAS strength of CON,[59] MFI,[58] and CHA[15,25] and zeolite framework type[13,16,22]) on hydrocarbon products selectivity has achieved in individual research. It needs to be emphasized that for the first time, by use of Equations (6) and (11) combined with characteristic dimension of framework (MISD and MFSD), feature size of targeted hydrocarbon molecules,[33] descriptors of acidity, for example, BAS density C_{BAS} and strength ξ_{H^+}, and reaction temperature can construct the primary panorama of shape-selective property of zeolite catalysts for MTH reactions.

Quantitative shape selectivity principle for MTH reactions Equation (6) provides unique opportunity to investigate the effect of multidimensional variables shown in Figure 5 on the selectivity of hydrocarbons. With this formula in hand, we can now formulate clear design rules to achieve ideal MTO catalysts maximizing ethylene, propylene and C_{4+} hydrocarbons selectivity, respectively. Figure 6A–C present the overview probability toward high selectivity of ethylene (>50%), propylene (>40%) and C_{4+} hydrocarbon species (>50%) for MTH reactions catalyzed by zeolite catalysts, and Figure 6D–F show corresponding BAS density, BAS strength and operating temperature to achieve goals shown in Figure 6A–C, respectively. In Figure 6A, zeolite catalysts with small 8 MR pores, for example, ERI, LEV, CHA, DDR and AFX frameworks, are potential candidate catalysts for high-selectivity production of ethylene. As discussed above, elevating reaction temperature (>673 K) can greatly promote the formation of ethylene. As indicated by Figure 6D, under high reaction temperature, as MFSD decreases, at least one of BAS density and BAS strength of zeolite need to be suitably decreased to avoid excessive formation of alkanes by hydrogen transfer reaction. To verify this concept, EU-7 zeolite (BIK topology) with small 8 MR pores (MFSD is 0.347 nm) and high BAS density (Si/Al ratio is 9.49) was synthesized. As shown in Figure S17, at the initial stage of MTH reactions, high value of
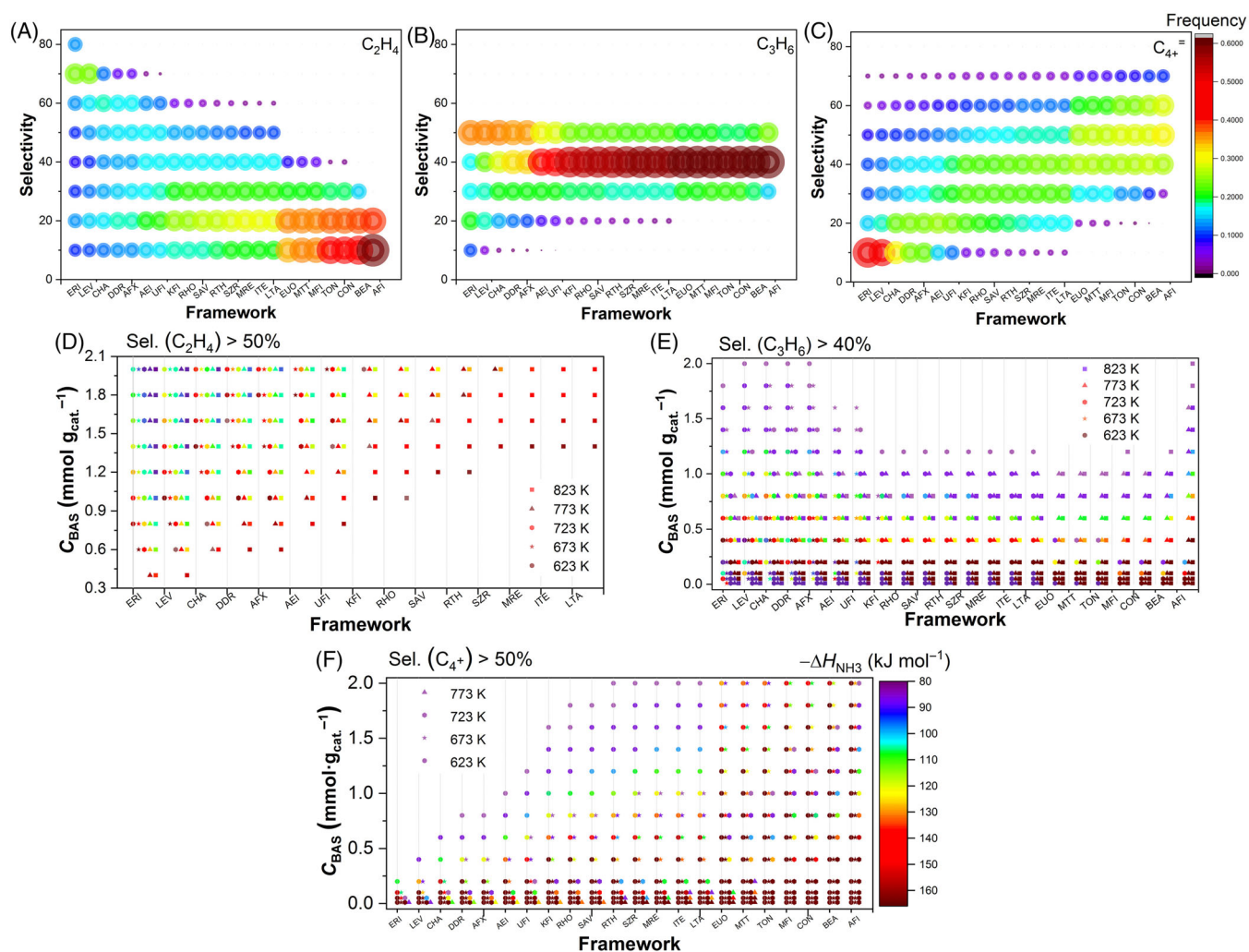
FIGURE 6 The probability distribution of (A) ethylene, (B) propylene, and (C) C_{4+} hydrocarbons selectivity for MTH reactions catalyzed by zeolite catalysts with diverse framework topologies and acidity properties at operating temperature range of 623–823 K. The optimized zeolite framework, BAS density, BAS strength, and operating temperature for the achievement of high selectivity of (D) ethylene (>50%), (E) propylene (>40%), and (F) C_{4+} hydrocarbons (>50%)

$Sel_{C_2^=}/Sel_{C_3^=}$ of EU-7 zeolite (~7.21) is achieved, which is accordance with predicted results of 7.88 by Equation (6). However, high BAS density and strength of EU-7 zeolite facilitate the hydrogen transfer of olefins, which leads to high selectivity of alkanes. The nature of thermodynamic equilibrium between olefin species within zeolite framework is favored for the propylene formation (Figure S24). In Figure 6B, high possibility for the achievement of high selectivity of propylene (>40%) is shown when implement of most zeolite catalysts for MTH reactions. Current research interests of MTP catalyst is mainly focused on the zeolite catalyst with large or medium pores, such as BEA and MFI[39,58,62] framework, and through decreasing BAS density or strength of these catalysts under elevated reaction temperature can further improve propylene selectivity. Interestingly, Figure 6B indicates that at moderate operating temperature (~623–673 K), zeolite framework with small pores, for example, ERI, LEV, CHA, DDR, AFX and AEI, and low BAS density, can be ascendant candidates for the achievement of higher propylene selectivity (>50%). This implies the important direction to the exploitation of zeolite with

small pores for high-performing MTP catalysts. Figure 6C,F represents the suitable properties of zeolite and reaction temperature for high selectivity of C_{4+} or hydrocarbons with long chain. Moderate reaction temperature (~623–673 K) and zeolite catalysts with medium or large pores, for example, AFI, BEA, CON, TON, MFI, MTT and EUO, and low BAS density are crucial to obtain high selectivity of heavier hydrocarbons. The application scope of Equation (6) is not limited to the zeolite catalysts shown in Figure 6, for given zeolite framework, Equation (6) can provide approximate probability distribution of hydrocarbons of MTH reactions catalyzed by such zeolites and primarily direct the optimization of acidity properties and operating temperature to achieve targeted olefins with high selectivity.

4 | CONCLUSIONS

In pursuit of high yield toward the hydrocarbon products converted from carbon resources by zeolite-based catalysis, despite enormous

endeavors in engineering zeolites with various framework topologies and acidity, an excellent performing zeolite catalysts are still quested. The understanding and description of shape selectivity of zeolite catalysis lies at the heart of improving a catalyst's performance, which can potentially liberate researcher from the empirical, labor-intensive tasks of synthesis, characterization, and reaction performance of zeolite catalysts. Herein, we constructed a quantitative principle of shape selectivity for zeolite catalysis using MTH reactions as model. Quantitative modeling indicates that to achieve maximized desired hydrocarbons selectivity, close coordination between framework topology, acidity properties (BAS density and strength) and operating temperature is essential. Such modeling is a very attractive methodology not only to search for the optimal combination of zeolite structure and reaction conditions that potentially outperform commercial MTH catalysts, but also extract fundamental knowledge about the molecular mechanism of shape selectivity. The key of shape-selective catalysis of zeolite is the competition of thermodynamic stability, preferential diffusion and favored secondary reactions between different hydrocarbons. According to the modeling, the thermodynamic stability of hydrocarbons within zeolite depends on the critical dimension of MISD of framework and molecular size, the competitive diffusion behavior between hydrocarbons lies on the feature size of MFSD and molecular size, and the favored secondary reactions, for example, β-scission reaction, of specific hydrocarbon is decided by its reaction kinetics (BAS density and strength) and residence time within framework. Hand in glove, MD simulations showed how zeolite framework decorated with BAS differentiate diffusion behavior between olefins and enhance the probability of secondary reactions of olefins with long chain at BAS. IRM technique showed the degree of β-scission of olefins with long chain is predominantly controlled by zeolite framework topology, which validated the results of modeling. Given the fact that zeolite catalysts often encounter local defects, which could introduce more variables for modeling and lead to more possibilities of performance of MTH reactions. We expect that the trends summarized by modeling here will provide primary and *in silico* screening rules for MTH catalysts.

AUTHOR CONTRIBUTIONS

Mingbin Gao: Conceptualization (lead); data curation (lead); formal analysis (lead); investigation (lead); methodology (lead); software (lead); validation (lead); visualization (lead); writing – original draft (lead). **Hua Li:** Formal analysis (supporting); methodology (equal). **Junyi Yu:** Formal analysis (supporting); software (supporting). **Mao Ye:** Funding acquisition (equal); project administration (equal); supervision (lead); writing – review and editing (lead). **Zhongmin Liu:** Funding acquisition (lead); project administration (lead); supervision (supporting); writing – review and editing (supporting).

ACKNOWLEDGMENTS

DATA AVAILABILITY STATEMENT

The data that support the findings of this study are available from the corresponding author upon reasonable request.

ORCID

Mingbin Gao https://orcid.org/0000-0002-7143-2658
Hua Li https://orcid.org/0000-0003-3291-7844
Mao Ye https://orcid.org/0000-0002-7078-2402

REFERENCES

1. Dusselier M, Davis ME. Small-pore zeolites: synthesis and catalysis. *Chem Rev*. 2018;118:5265-5329.
2. Li Y, Yu J. Emerging applications of zeolites in catalysis, separation and host–guest assembly. *Nat Rev Mater*. 2021;6:1156-1174.
3. Vogt ETC, Weckhuysen BM. Fluid catalytic cracking: recent developments on the grand old lady of zeolite catalysis. *Chem Soc Rev*. 2015; 44:7342-7370.
4. Tian P, Wei Y, Ye M, Liu Z. Methanol to olefins (MTO): from fundamentals to commercialization. *ACS Catal*. 2015;5:1922-1938.
5. Smit B, Maesen TLM. Towards a molecular understanding of shape selectivity. *Nature*. 2008;451:671-678.
6. Olsbye U, Svelle S, Bjørgen M, et al. Conversion of methanol to hydrocarbons: how zeolite cavity and pore size controls product selectivity. *Angew Chem Int Ed*. 2012;51:5810-5831.
7. Keil FJ. Methanol-to-hydrocarbons: process technology. *Microporous Mesoporous Mater*. 1999;29:49-66.
8. Keil FJ. Molecular modelling for reactor design. *Annu Rev Chem Biomol Eng*. 2018;9:201-227.
9. Ye G, Zhou X, Yuan W, Coppens MO. Probing pore blocking effects on multiphase reactions within porous catalyst particles using a discrete model. *AIChE J*. 2015;62:451-460.
10. Bukowski BC, Keil FJ, Ravikovitch PI, Sastre G, Snurr RQ, Coppens M-O. Connecting theory and simulation with experiment for the study of diffusion in nanoporous solids. *Adsorption*. 2021;27:683-760.
11. Yarulina I, Chowdhury AD, Meirer F, Weckhuysen BM, Gascon J. Recent trends and fundamental insights in the methanol-to-hydrocarbons process. *Nat Catal*. 2018;1:398-411.
12. Lehmann T, Seidel-Morgenstern A. Thermodynamic appraisal of the gas phase conversion of ethylene or ethanol to propylene. *Chem Eng J*. 2014;242:422-432.
13. Kang JH, Alshafei FH, Zones SI, Davis ME. Cage-defining ring: a molecular sieve structural indicator for light olefin product distribution from the methanol-to-olefins reaction. *ACS Catal*. 2019;9: 6012-6019.
14. Ferri P, Li C, Paris C, et al. Chemical and structural parameter connecting cavity architecture, confined hydrocarbon pool species, and MTO product selectivity in small-pore cage-based zeolites. *ACS Catal*. 2019;9:11542-11551.
15. Ferri P, Li C, Millán R, et al. Impact of zeolite framework composition and flexibility on methanol-to-olefins selectivity: confinement or diffusion? *Angew Chem Int Ed*. 2020;59:19708-19715.
16. Teketel S, Lundegaard LF, Skistad W, et al. Morphology-induced shape selectivity in zeolite catalysis. *J Catal*. 2015;327:22-32.
17. Bhawe Y, Moliner-Marin M, Lunn JD, Liu Y, Malek A, Davis M. Effect of cage size on the selective conversion of methanol to light olefins. *ACS Catal*. 2012;2:2490-2495.
18. Li J, Wei Y, Chen J, et al. Cavity controls the selectivity: insights of confinement effects on MTO reaction. *ACS Catal*. 2015;5:661-665.

19. Pinilla-Herrero I, Olsbye U, Márquez-Álvarez C, Sastre E. Effect of framework topology of SAPO catalysts on selectivity and deactivation profile in the methanol-to-olefins reaction. *J Catal*. 2017;352:191-207.

20. Kang JH, Walter R, Xie D, et al. Further studies on how the nature of zeolite cavities that are bounded by small pores influences the conversion of methanol to light olefins. *ChemPhysChem*. 2018;19:412-419.

21. Li C, Paris C, Martínez-Triguero J, Boronat M, Moliner M, Corma A. Synthesis of reaction-adapted zeolites as methanol-to-olefins catalysts with mimics of reaction intermediates as organic structure-directing agents. *Nat Catal*. 2018;1:547-554.

22. Ferri P, Li C, Paris C, et al. The limits of the confinement effect associated to cage topology on the control of the MTO selectivity. *ChemCatChem*. 2021;13:1578-1586.

23. Noh G, Shi Z, Zones SI, Iglesia E. Isomerization and β-scission reactions of alkanes on bifunctional metal-acid catalysts: consequences of confinement and diffusional constraints on reactivity and selectivity. *J Catal*. 2018;368:389-410.

24. DeLuca M, Janes C, Hibbitts D. Contrasting Arene, alkene, diene, and formaldehyde hydrogenation in H-ZSM-5, H-SSZ-13, and H-SAPO-34 frameworks during MTO. *ACS Catal*. 2020;10:4593-4607.

25. Wang C-M, Brogaard RY, Weckhuysen BM, Nørskov JK, Studt F. Reactivity descriptor in solid acid catalysis: predicting turnover frequencies for propene methylation in zeotypes. *J Phys Chem Lett*. 2014;5:1516-1521.

26. Brogaard RY, Wang C-M, Studt F. Methanol–alkene reactions in zeotype acid catalysts: insights from a descriptor-based approach and microkinetic modeling. *ACS Catal*. 2014;4:4504-4509.

27. Kärger J, Binder T, Chmelik C, et al. Microimaging of transient guest profiles to monitor mass transfer in nanoporous materials. *Nat Mater*. 2014;13:333-343.

28. Hendriks FC, Meirer F, Kubarev AV, et al. Single-molecule fluorescence microscopy reveals local diffusion coefficients in the pore network of an individual catalyst particle. *J Am Chem Soc*. 2017;139:13632-13635.

29. Beerdsen E, Dubbeldam D, Smit B. Understanding diffusion in nanoporous materials. *Phys Rev Lett*. 2006;96:044501.

30. Skoulidas AI, Sholl DS. Transport diffusivities of CH4, CF4, He, Ne, Ar, Xe, and SF6 in silicalite from atomistic simulations. *J Phys Chem B*. 2002;106:5058-5067.

31. Verploegh RJ, Nair S, Sholl DS. Temperature and loading-dependent diffusion of light hydrocarbons in ZIF-8 as predicted through fully flexible molecular simulations. *J Am Chem Soc*. 2015;137:15760-15771.

32. Cnudde P, Demuynck R, Vandenbrande S, Waroquier M, Sastre G, Speybroeck VV. Light olefin diffusion during the MTO process on H-SAPO-34: a complex interplay of molecular factors. *J Am Chem Soc*. 2020;142:6007-6017.

33. Gao M, Li H, Ye M, Liu Z. An approach for predicting intracrystalline diffusivities and adsorption entropies in nanoporous crystalline materials. *AIChE J*. 2020;66:e16991.

34. Keil Frerich J, Krishna R, Coppens M-O. Modeling of diffusion in zeolites. *Rev Chem Eng*. 2000;16:71-197.

35. Liu Z, Yuan J, van Baten JM, et al. Synergistically enhance confined diffusion by continuum intersecting channels in zeolites. *Sci Adv*. 2021;7:eabf0775.

36. Treacy MMJ, Foster MD. Packing sticky hard spheres into rigid zeolite frameworks. *Microporous Mesoporous Mater*. 2009;118:106-114.

37. Ye G, Wang H, Zhou X, Keil FJ, Coppens M-O, Yuan W. Optimizing catalyst pore network structure in the presence of deactivation by coking. *AIChE J*. 2019;65:e16687.

38. Guo Z, Li X, Hu S, Ye G, Zhou X, Coppens M-O. Understanding the role of internal diffusion barriers in Pt/Beta zeolite catalyzed isomerization of n-heptane. *Angew Chem Int Ed*. 2020;59:1548-1551.

39. Yarulina I, De Wispelaere K, Bailleul S, et al. Structure–performance descriptors and the role of Lewis acidity in the methanol-to-propylene process. *Nat Chem*. 2018;10:804-812.

40. Remi JCS, Lauerer A, Chmelik C, et al. The role of crystal diversity in understanding mass transfer in nanoporous materials. *Nat Mater*. 2016;15:401-406.

41. Zimmermann NER, Balaji SP, Keil FJ. Surface barriers of hydrocarbon transport triggered by ideal zeolite structures. *J Phys Chem C*. 2012;116:3677-3683.

42. Gao M, Li H, Yang M, et al. Direct quantification of surface barriers for mass transfer in nanoporous crystalline materials. *Commun Chem*. 2019;2:43-52.

43. Myers AL, Prausnitz JM. Thermodynamics of mixed-gas adsorption. *AIChE J*. 1965;11:121-127.

44. Baur R, Krishna R. The effectiveness factor for zeolite catalysed reactions. *Catal Today*. 2005;105:173-179.

45. Peng P, Gao X-H, Yan Z-F, Mintova S. Diffusion and catalyst efficiency in hierarchical zeolite catalysts. *Natl Sci Rev*. 2020;7:1726-1742.

46. Garcia SF, Weisz PB. Effective diffusivities in zeolites 1. Aromatics in ZSM-5 crystals. *J Catal*. 1990;121:294-311.

47. Müller S, Liu Y, Kirchberger FM, Tonigold M, Sanchez-Sanchez M, Lercher JA. Hydrogen transfer pathways during zeolite catalyzed methanol conversion to hydrocarbons. *J Am Chem Soc*. 2016;138:15994-16003.

48. Westgård Erichsen M, Svelle S, Olsbye U. H-SAPO-5 as methanol-to-olefins (MTO) model catalyst: towards elucidating the effects of acid strength. *J Catal*. 2013;298:94-101.

49. Hua J, Dong X, Wang J, et al. Methanol-to-olefin conversion over small-pore DDR zeolites: tuning the propylene selectivity via the olefin-based catalytic cycle. *ACS Catal*. 2020;10:3009-3017.

50. Wilson S, Barger P. The characteristics of SAPO-34 which influence the conversion of methanol to light olefins. *Microporous Mesoporous Mater*. 1999;29:117-126.

51. Tranca DC, Keil FJ, Tranca I, et al. Methanol oxidation to formaldehyde on VSiBEA zeolite: a combined DFT/vdW/transition path sampling and experimental study. *J Phys Chem C*. 2015;119:13619-13631.

52. Liu Z, Zhou J, Tang X, et al. Dependence of zeolite topology on alkane diffusion inside nano-channels. *AIChE J*. 2020;66:e16269.

53. Gao M, Li H, Liu W, et al. Imaging spatiotemporal evolution of molecules and active sites in zeolite catalyst during methanol-to-olefins reaction. *Nat Commun*. 2020;11:3641-3652.

54. Hutter J, Iannuzzi M, Schiffmann F, VandeVondele J. cp2k: atomistic simulations of condensed matter systems. *WIREs Comput Mol Sci*. 2014;4:15-25.

55. Allotta PM, Stair PC. Time-resolved studies of ethylene and propylene reactions in zeolite H-MFI by in-situ fast IR heating and UV Raman spectroscopy. *ACS Catal*. 2012;2:2424-2432.

56. Signorile M, Rojo-Gama D, Bonino F, Beato P, Svelle S, Bordiga S. Topology-dependent hydrocarbon transformations in the methanol-to-hydrocarbons reaction studied by operando UV-Raman spectroscopy. *Phys Chem Chem Phys*. 2018;20:26580-26590.

57. Alshafei FH, Park Y, Zones SI, Davis ME. Methanol-to-OlefinsCatalysis on ERI-type molecular sieves: towards enhancing ethylene selectivity. *J Catal*. 2021;404:620-633.

58. Lin L, Fan M, Sheveleva AM, et al. Control of zeolite microenvironment for propene synthesis from methanol. *Nat Commun*. 2021;12:822.

59. Yoshioka M, Yokoi T, Tatsumi T. Development of the CON-type aluminosilicate zeolite and its catalytic application for the MTO reaction. *ACS Catal*. 2015;5:4268-4275.

60. Deimund MA, Harrison L, Lunn JD, et al. Effect of heteroatom concentration in SSZ-13 on the methanol-to-olefins reaction. *ACS Catal.* 2016;6:542-550.
61. Sun Q, Wang N, Bai R, et al. Mesoporogen-free synthesis of hierarchical SAPO-34 with low template consumption and excellent methanol-to-olefin conversion. *ChemSusChem.* 2018;11:3812-3820.
62. Khare R, Liu Z, Han Y, Bhan A. A mechanistic basis for the effect of aluminum content on ethene selectivity in methanol-to-hydrocarbons conversion on HZSM-5. *J Catal.* 2017;348:300-305.

SUPPORTING INFORMATION

Additional supporting information can be found online in the Supporting Information section at the end of this article.